Acta Materialia 273 (2024) 119914

Contents lists available at ScienceDirect

Acta Materialia

journal homepage: www.elsevier.com/locate/actamat

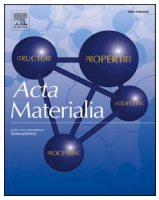

Microcantilever investigation of slow crack growth and crack healing in aluminium oxide

Jiawei Jiang [a], Simone Falco [b], Siyang Wang [c], Finn Giuliani [c], Richard I Todd [a,*]

[a] Department of Materials, University of Oxford, Oxford OX1 3PH, United Kingdom
[b] Department of Engineering Science, University of Oxford, Oxford OX1 3PJ, United Kingdom
[c] Department of Materials, Imperial College, London SW7 2AZ, United Kingdom

ARTICLE INFO

Keywords:
Aluminium oxide
Fracture toughness
Slow crack growth
Environment-assisted cracking
Microcantilevers
Crack healing

ABSTRACT

Slow crack growth (SCG) plays an important role in the fracture of ceramics and glasses. A full understanding of the long term reliability of ceramic components therefore requires knowledge not only of fracture toughness (K_c) but also characteristics of SCG such as the threshold stress intensity factor (K_0) of individual microstructural features. Previous investigations have been limited by the small scale of the microstructure and low crack growth rates involved. Here, the stress intensity factors for crack propagation K_p in sapphire were measured continuously under stable crack growth using chevron-notched microcantilevers, in air and in vacuum. K_p in vacuum was considered close to the fracture toughness K_c, with a value of 2.8 ± 0.1 MPa $m^{1/2}$ for the a-plane of sapphire. K_p in air at 54 % relative humidity was reduced substantially by moisture-assisted SCG to around 1.7 MPa $m^{1/2}$ and, with crack velocities of ~20 nm/s, was considered to be close to K_0. Cyclic loading in vacuum enabled quantitative measurements to be made during repeated crack growth and healing for the first time. Cracks healed up along their full length when unloaded but exhibited severe degradation of toughness on reloading. The toughness fell from 2.8 MPa $m^{1/2}$ on the *a*-plane of pristine sapphire to 1.6 MPa $m^{1/2}$ after one healing cycle and to successively lower values after further cycles. This technique offers a powerful method of investigating SCG and crack healing at the microstructural scale in different environments, with greater accuracy and on shorter timescales than can be achieved in macroscopic tests.

1. Introduction

Ceramic materials have been used extensively in engineering for decades [1–6] because of their high hardness, low density compared to metals, high compressive strength, and good thermal and chemical stability. However, the brittle nature of ceramics often restricts their performance upon loading. A good understanding of their fracture behaviour is thus of great importance.

Despite the extensive investigation of the fracture of ceramics using macroscopic specimens, knowledge of their fracture characteristics at the microstructural scale is limited. Studying the fracture response of microstructural components is essential for a full understanding of the fracture of the bulk materials and the development of predictions of failure of polycrystalline ceramics, especially in terms of crack initiation and propagation mechanisms. Moreover, accurate measurement at the microscale could not only allow for the improvement of corresponding properties *via* mechanistically informed microstructural engineering, but also enable the investigation of certain characteristics that are difficult to study using macroscopic tests, such as slow crack growth (SCG) [7].

Beyond its potential consequences in measurement of fracture toughness K_c in laboratories, in which the aim is usually to avoid its effects, SCG plays an important role in engineering design and materials performance in real components. This is because most applications of engineering ceramics involve timescales and environments under which SCG, rather than the more commonly studied fast fracture characteristics, can lead to failure. This suggests that the measurement of the threshold value for SCG K_0, below which crack growth does not occur, should be more important than K_c for ensuring the long term reliability of ceramics.

SCG is exacerbated, particularly in oxide ceramics, by moisture in the testing environment, which interacts with the atomic bonds at the crack tip to assist in its propagation. In toughness testing, this potentially results in a stress intensity factor K at failure that is below the critical value

* Corresponding author.
E-mail address: richard.todd@materials.ox.ac.uk (R.I. Todd).

https://doi.org/10.1016/j.actamat.2024.119914
Received 4 February 2024; Received in revised form 8 April 2024; Accepted 10 April 2024
Available online 14 April 2024

in vacuum or other inert environment, K_c [8,9]. For this reason, the phenomenon is often called "subcritical" crack growth but this is potentially misleading, as is described below. The phenomenon has been extensively investigated using macroscopic specimens [10–14] back to the 1960s, but investigation has only recently been extended to the microscopic scale [15,16].

SCG is generally categorised in terms of the regions [17–21] shown in Fig. 1. In *Region I*, the crack begins to propagate only once the stress intensity factor reaches a threshold value K_0; no propagation is considered to occur when K is below K_0. The crack growth velocity above K_0 depends strongly on the stress intensity factor and is controlled by the chemical reaction rate involving atmospheric moisture at the crack tip. The relationship between the crack velocity (v) and stress intensity factor (K) is generally described by a power law, $v = AK^n$, where A and n are constants depending on the material and specific testing environment [7].

In *Region II,* at higher K, the transport rate of the moisture diffusing from the environment to the crack tip becomes rate-controlling. This results in a quasi-plateau, where the crack advances at an almost constant rate, independent of K.

In *Region III*, the chemical attack of the moisture at the crack tip is no longer the rate-controlling process and the crack growth velocity increases significantly, leading to fast fracture at a rate eventually limited by the elastic response of the material, shown in Fig. 1 at a stress intensity factor $K_{c(f)}$. This if often regarded as the "true" fracture toughness, though largely for experimental reasons: stable, low velocity crack growth is difficult to achieve, and testing at high rate, to achieve fast fracture, is the most common method of avoiding the atmospheric effects involved in Regions 0-II, alternatives such as testing in silicone oil [16,22] or inert gas [23,24] to exclude moisture being less convenient. However, as has been emphasised by Olagnon et al. [20], within the thermodynamic framework of Griffith's theory of brittle fracture, the fundamental measure of toughness in an inert atmosphere or vacuum should be the threshold or equilibrium value shown as $K_{c(G)}$ in Fig. 1, where the mechanical energy release rate G is equal to the crack resistance energy R. At this point the crack tip is on the point of extension but its velocity is zero; above $K_{c(G)}$ the crack propagates (Region III) and below it the crack does not get longer and may even heal up if there is no mechanical or chemical impediment to this process. There is thus no "subcritical" crack growth in an inert environment, and Region III represents the $v - K$ relationship *above* the critical point. In practice, given the difficulty in making accurate toughness measurements, the difference between $K_{c(G)}$ and $K_{c(f)}$ is usually considered sufficiently small for it to be within experimental error and for this reason, the stress intensity factor for crack propagation in vacuum or other inert environment in this work will be referred to as K_c unless there is a specific reason to distinguish the two values above. However, it is noted that despite its fundamental significance, there are very few attempts in the literature to actually measure the threshold $K_{c(G)}$ for Region III or to investigate crack healing below it, presumably because of the experimental difficulties involved.

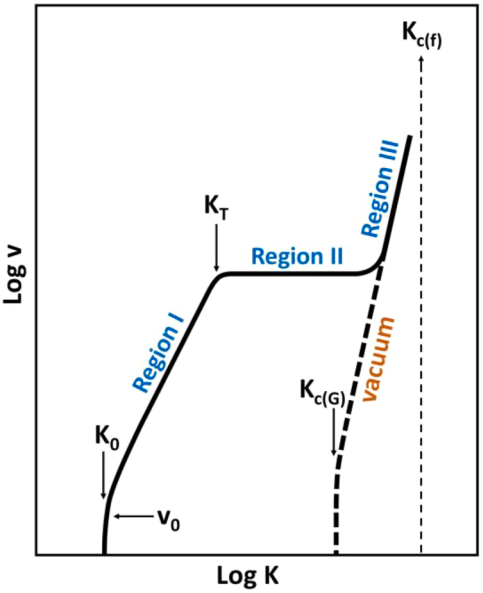

Fig. 1. Schematic of crack velocity (v) as a function of stress intensity factor (K) in SCG.

In a reactive environment, K_0 is the stress intensity factor at which $G = R_E$, the crack resistance taking account of the additional chemical energy involved in crack growth [8,9] and is the fundamental counterpart to $K_{c(G)}$ in an inert environment. As with Region III, the SCG response in Regions I and II is really the v-K response *above* this critical point and in this scientific sense, there is again no "subcritical" crack growth, the traditional name simply referring to the fact that K_0 is less than K_c for reasons that are now well understood.

In this work, the term K_p will be used in the Results section for the measured stress intensity factor at which a crack propagated under a particular experimental condition (environment, fracture plane, crack velocity etc.). The experimental K_p values will then be associated with the various physically meaningful stress intensity factors described above in the Discussion section.

Turning now to the experimental background to this work, in the 1960s, a series of fracture tests was conducted by Wiederhorn [17,23,25] to reveal the effect of SCG on ceramics using macroscopic specimens. This laid the groundwork for future research in the construction of $v - K$ curves [8]. Later on, further investigation on SCG was carried out at the macroscopic scale by several other researchers, with some of the results on sapphire compared by Salem [24] along with his own data. The SCG results are highly scattered, at least partly due to the difficulty of measuring the very low crack growth rates involved ($\sim 10^{-9}$ to 10^{-4} m s^{-1}) with macroscopic specimens on the laboratory time scale. Salem's [24] own experiments on single-edge pre-cracked beams suggest a fracture toughness value of 2.31 ± 0.12 MPa $m^{1/2}$ for the a-plane of sapphire based on measurements conducted in dry nitrogen, while the threshold stress intensity factor for crack propagation in water is significantly lower (1.95 ± 0.03 MPa $m^{1/2}$ for the a-plane). Data collected on the m-plane were close to those from the a-plane.

Considering these difficulties with the very slow crack rates involved in SCG, it is understandable that attempts have been made to investigate the effect of SCG on brittle fracture using microscopic specimens in the past decade, during which micromechanical testing methods have developed. Norton et al. [16] tested sapphire microcantilevers with straight-through notches in air, water and silicone oil. With corrections for notch bluntness and focused ion beam (FIB) implantation-induced residual stresses at notch tips, the stress intensity values for crack propagation K_p on the m-plane of sapphire were reported to be much lower for tests conducted in air (1.5 ± 0.2 MPa $m^{1/2}$) than in oil (3.5 ± 0.2 MPa $m^{1/2}$), with even lower K_p values from specimens tested in water (0.9 ± 0.2 MPa $m^{1/2}$). Although the corrections mentioned introduce some uncertainty to the absolute values, the results show clearly that the effect of moisture on the fracture of microscopic specimens can be significant. Analysis also showed that K_p measured in air by these tests should be close to K_0 for that environment, while that measured in oil should be close to K_c.

Testing with stable crack growth can potentially avoid the problems of blunt notches and FIB damage mentioned above. Mueller et al. [26] applied the chevron notch configuration to microcantilevers of nanocrystalline alumina and stable crack propagation was achieved. Despite the fact that the measurement was conducted in air, it was reported that the effect of SCG was absent in their tests [15] and the measured K_p (2.34 ± 0.15 MPa $m^{1/2}$) was concluded to represent the fracture toughness K_c. This conclusion was on the basis (i) that their K_p values are close to

measurements of K_c for similar materials [26] and (ii) that a compliance condition developed by Žagar et al. [15] was satisfied by the tests. However, this later paper of Žagar et al. [15] also concludes that SCG should have affected the results of such tests and that loading rates several orders of magnitude higher than were used would be necessary to avoid its effect. The authors of Ref. [15] were unable to explain this contradiction and no tests were conducted in inert atmosphere for comparison. There is thus some uncertainty in the applicability of chevron notched microcantilevers in the measurement of either the SCG characteristics of ceramics, or the inert fracture toughness.

In view of the contradiction between the work of Norton et al. [16], in which the effects of moisture-induced SCG are clear, and Mueller et al. [26], in which they are apparently absent and where there are some unresolved problems, research is needed to investigate whether micro-cantilever tests can be used to characterise SCG or not. In the present study, measurements of K_p in sapphire were made using chevron-notched microcantilevers similar to those used by Mueller et al. [26]. In a further development to the testing method, the compliance of the specimen during crack growth was used to deduce the crack length throughout the test. This allows K_p to be measured as the crack evolves, from the zone beyond the notch tip, when the crack front is atomically sharp and substantially free from the effects induced by FIB milling (such as ion implantation [16] and residual stresses [27] at the notch tip, notch bluntness [28,29], and the nature and morphology of the notch surface [27]). It also enables the crack tip velocities corresponding to the K_p measurements to be deduced so that the regime of crack growth can be put into the context of previous, macroscopic investigations of SCG. In addition, monotonic loading was performed here in both air and vacuum, i.e. in environments respectively containing and excluding moisture, to provide an unambiguous assessment of the effect of moisture on crack growth in chevron-notched microcantilevers. Finally, cyclic loading in vacuum with low crack growth rate enabled quantitative investigation of the near-threshold toughness value in vacuum $K_{c(G)}$ and of crack healing and repropagation in sapphire [30–32].

2. Experimental

2.1. Materials and sample preparation

c-plane (0001) sapphire ($5 \times 5 \times 0.5\ mm^3$, purity 99.995 %, AdValue Technology, United States) was chosen for this investigation. The sample surfaces were tribochemically polished using silica slurry by the supplier to have a surface roughness (Ra) $\leq$ 0.2 nm. The substrate was mounted to a SEM pin stub using silver paint which was followed by carbon coating (Edwards E306, Sweden) to gain conductivity.

Crystal orientations were identified using EBSD (Zeiss Merlin-Bruker), with the a- and m-axes marked on the sapphire surface using FIB to guide the subsequent production of cantilevers.

The cantilevers were manufactured with pentagonal cross sections and thin chevron notches, as illustrated in Fig. 2. During testing, the beam bends under the load P, initiating a Mode I crack from the apex of the ligament, which is a distance a_0 from the beam top surface. While the crack propagates, it grows to a length $\alpha = a\text{-}a_0$ and width $b = W\alpha/(a_1\text{-}a_0)$.

Microcantilevers were manufactured using FIB (Zeiss Auriga FIB-SEM, Germany) [16]. The final and most crucial step was to mill the chevron notch. A 50 pA beam current was applied, with the notch shaped to have the apex angled at about 90°. In order to minimise the effect of the Gaussian ion beam spot profile [33], the apex of the notch was located well below the top surface of the beam, ensuring $a_0/H \geq 0.4$ as suggested by Mueller et al. [26]. High-resolution SEM images of the cantilevers were taken before and after failure for measuring the beam dimensions.

The sapphire specimens were annealed in argon in a tube furnace (Carbolite STF 16/60/180) at 1100 °C for 1 h, with 3 °C/min heating and cooling rate. This step was for removing the residual stresses introduced by FIB in the cantilevers, especially at the notch.

2.2. Microcantilever testing

For the tests in air, the microcantilevers were tested using an *ex-situ* nanoindenter (G200, Keysight Technologies, USA) coupled with a diamond Berkovich nanoindenter tip (Synton-MDP, Switzerland). The cantilever was loaded under pseudo-displacement control mode with a nominal displacement rate of 2 nm/s until failure, with a data recording time interval of 0.2 s. The relative humidity of the testing environment in air was 53.6 ± 6.8 % at 16℃ (measured using Omegaette HH311, Omega).

For the tests in vacuum, the cantilevers were tested using an intrinsically displacement-controlled *in-situ* SEM nanoindenter (Alemnis, Switzerland) within a FEI Quanta 650 SEM. The indenter stage was 20° pre-tilted in order to enable the visibility of the sides of cantilevers. A cube corner diamond nanoindenter tip (Synton-MDP, Switzerland) was used to load the cantilevers. The tests were performed under the displacement-controlled mode, enabled by the piezoelectric transducer in the Alemnis nanoindenter. A displacement rate of 2 nm/s was applied during loading and the unloading rate in cyclic loading was 20 nm/s. A series of SEM images was taken every 2 s during the cantilever bending

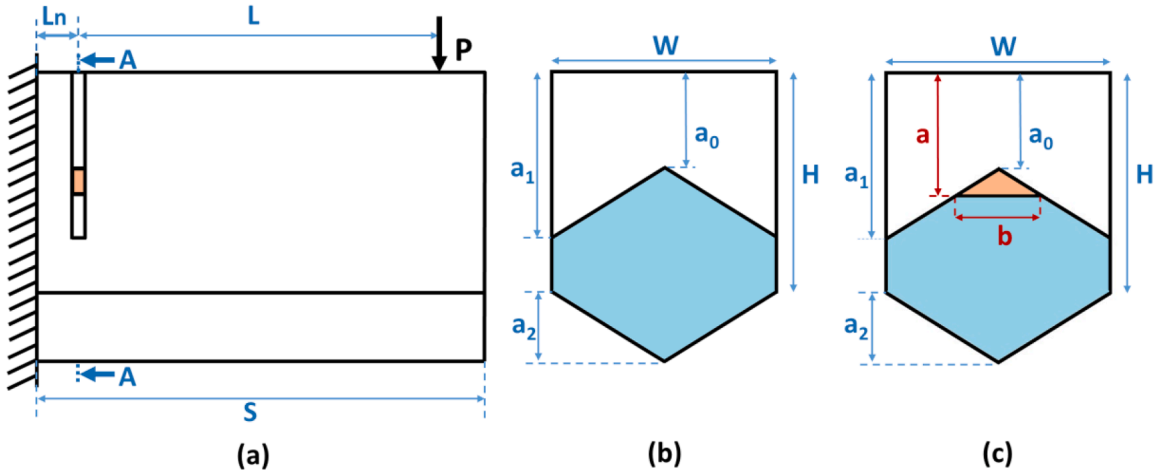

Fig. 2. Schematic of the chevron-notched cantilevers. (a) The side view of the cantilever. (b) Cross section of the notch as manufactured, prior to cracking. (c) Cross section of the notch during crack propagation. The blue area is the ligament connecting the parts of the system on either side of the notch. The orange regions in (a) and (c) indicate the parts of the ligament through which the crack has grown, and is therefore wider in (a) than the crack itself.

process, with a SEM frame scan time of 1.6 s.

The load drift rate was evaluated by $(P_f - P_0)/t_f$, where P_f is the raw load after failure reported by the nanoindenter when the cantilever is separated from the indenter tip, P_0 is the load immediately before the test and is therefore equal to 0, t_f is the total loading time.

For the monotonic loading tests, the displacement drift rate was evaluated by correcting the compliance of the cantilever during elastic bending to the compliance interpreted from the corresponding numerical model at 0 crack extension. For the cyclic loading tests, the displacement drift rate was evaluated based on the recorded timeline and the displacement drift between the starting point (i.e. $P = 0$) of each two consecutive loading cycles. This gave a value close to that evaluated based on the compliance of the cantilever from numerical models and therefore validated the above procedure for monotonic loading tests.

2.3. Analysis of fracture results

Stress intensity factors were calculated by combining an analytical method similar to that of Munz et al. [34] with finite element analysis of specimen compliance. The mechanical energy release rate, G, of a beam with an applied force P is given by:

$$G = -\frac{dU_M}{dA} = \frac{P^2}{2b}\frac{dC}{d\alpha} = \frac{P^2}{2H^2bE}\frac{dC'}{d\alpha'} \tag{1}$$

where U_M is the mechanical energy of the system, A is the cracked area, $dA = b{\cdot}d\alpha$, and C is the compliance. α' and C' are dimensionless values of the crack length and compliance, defined as:

$$\alpha' = \frac{\alpha}{H} \tag{2}$$

$$C' = CEH \tag{3}$$

where E is the effective modulus accounting for anisotropy [35], which is taken to be the Young's modulus in the basal plane $= 1/s_{11}$ in the present study.

The stress intensity factor, K, can then be calculated:

$$K = \sqrt{GE} = \frac{P}{H\sqrt{b}}\left(\frac{1}{2}\frac{dC'}{d\alpha'}\right)^{\frac{1}{2}} = \frac{P}{H\sqrt{W}}\left(\frac{1}{2}\frac{a_1 - a_0}{\alpha}\frac{dC'}{d\alpha'}\right)^{\frac{1}{2}} \tag{4}$$

Writing the dimensionless factor $\left(\frac{1}{2}\frac{a_1-a_0}{\alpha}\frac{dC'}{d\alpha}\right)^{\frac{1}{2}}$ as $Y(\alpha')$, Eq. (4) becomes:

$$K = \frac{P}{H\sqrt{W}}Y(\alpha') \tag{5}$$

The compliances of particular cantilevers at different crack lengths were calculated using numerical simulation (see below), which gave a set of data points of C' vs. α' for each beam. The data were fitted by a fifth-order polynomial.

$$C' = B_0 + B_1\alpha' + B_2\alpha'^2 + B_3\alpha'^3 + B_4\alpha'^4 + B_5\alpha'^5 \tag{6}$$

The value of $dC'/d\alpha'$ in $Y(\alpha')$ can be derived as

$$\frac{dC'}{d\alpha'} = B_1 + 2B_2\alpha' + 3B_3\alpha'^2 + 4B_4\alpha'^3 + 5B_5\alpha'^4 \tag{7}$$

thus enabling the calculation of $Y(\alpha')$, and hence K for each combination of crack length and load *via* Eq. (5).

The derived $Y(\alpha')$ points were fitted with a fifth-order polynomial:

$$Y(\alpha') = N_0 + N_1\alpha' + N_2\alpha'^2 + N_3\alpha'^3 + N_4\alpha'^4 + N_5\alpha'^5 \tag{8}$$

$Y(\alpha')$ exhibits a minimum value at a specific crack length α'_c which also gives a minimum value to K for a given P. The values of α'_c and $Y(\alpha'_c)$ can be obtained by differentiation of (8). Crack growth is therefore stable under load-controlled conditions for $\alpha' < \alpha'_c$ The traditional method of analysing chevron notch results, used by Mueller et al. [26], is to use the load applied at the point of instability P_c to calculate the corresponding stress intensity factor K_p at the critical crack length α_c:

$$K_{p\ (\alpha_c)} = \frac{P_c}{H\sqrt{W}}Y(\alpha'_c) \tag{9}$$

However, knowing the load point displacement δ, the instantaneous stress intensity factor to propagate the crack, K_p, can also be calculated at any point during stable crack growth as follows. Since the beams are elastic, the compliance $C(\alpha)$ at each measurement condition is $\delta(\alpha)/P(\alpha)$. α' can then be back calculated using Eq. (6), which enables the calculation in turn of $Y(\alpha')$ and hence $K_p(\alpha')$ using Eqs. (8) and (5) respectively. The present work uses this method to calculate K_p continuously during crack propagation.

Now knowing the instantaneous crack lengths α ($=\alpha' H$) from the compliance, coupled with the corresponding times at measurement, the crack tip velocity, v, can also be calculated as $d\alpha/dt$.

2.4. Development and optimisation of numerical models

The complexity of the deformation of the notched beam prevents the analytical calculation of the compliance of the structure as the crack propagates. Numerical models were therefore developed in the commercial software LS-Dyna to interpret the experimental results. The dimensions measured from SEM pictures were used to build a set of Finite Element (FE) models for each cantilever beam, inserting cracks of increasing length to calculate the evolution of the compliance as the crack propagates. Part of the root support was included in the models for a more accurate evaluation of the compliance. The elastic models were made to be fully anisotropic using the following values for the components of the stiffness tensor [36]: c_{11}= c_{22}=497 GPa, c_{12}=163 GPa, c_{13}=c_{23}=116 GPa, c_{14}=22 GPa, c_{33}=501 GPa, c_{44}=147 GPa.

The cross section was discretised mostly with quad elements, with the cross-sectional mesh extruded to form a 3D mesh consisting predominantly of hexahedral elements with a small percentage (<1 %) of pentahedron elements. In order to mimic the real nanoindenter tip and to avoid local deformation caused by stress concentration in the model, a pressure load was applied on a square area of 0.8 μm side length, centred at the experimentally determined loading point.

Although the importance of validating the reliability of numerical models is generally recognised in the field of numerical simulations [37], it often receives insufficient attention in the experimental literature, despite the wide application of numerical models for assisting empirical analysis. The present study shows the necessity of ensuring the reliability of numerical models as it affects directly the accuracy of fracture toughness values. In order to ensure the accuracy of simulation results, the models were optimised in terms of mesh size and the compliant built-in root based on the following investigation.

(a) Graded mesh size

The effect of mesh size was verified by comparing compliance results interpreted from models meshed with different element sizes. As shown in Fig. 3*a*, it was found that the mesh size needed to be fine enough ($\leq$ 0.4 μm) to avoid underestimation of compliances. Therefore, in order to achieve an ideal balance between high accuracy and computational time, graded meshing with mesh size $\leq$ 0.05 μm at the notch and $\leq$ 0.4 μm away from the notch was applied in constructing numerical models in the present study.

(b) Compliant beam root

As the deformation of the beam root contributes to the deflection of the cantilever [38], both the numerical models without beam root and the analytical theories (i.e. Euler-Bernoulli and Timoshenko beam theories) underestimated the beam compliance by a significant amount

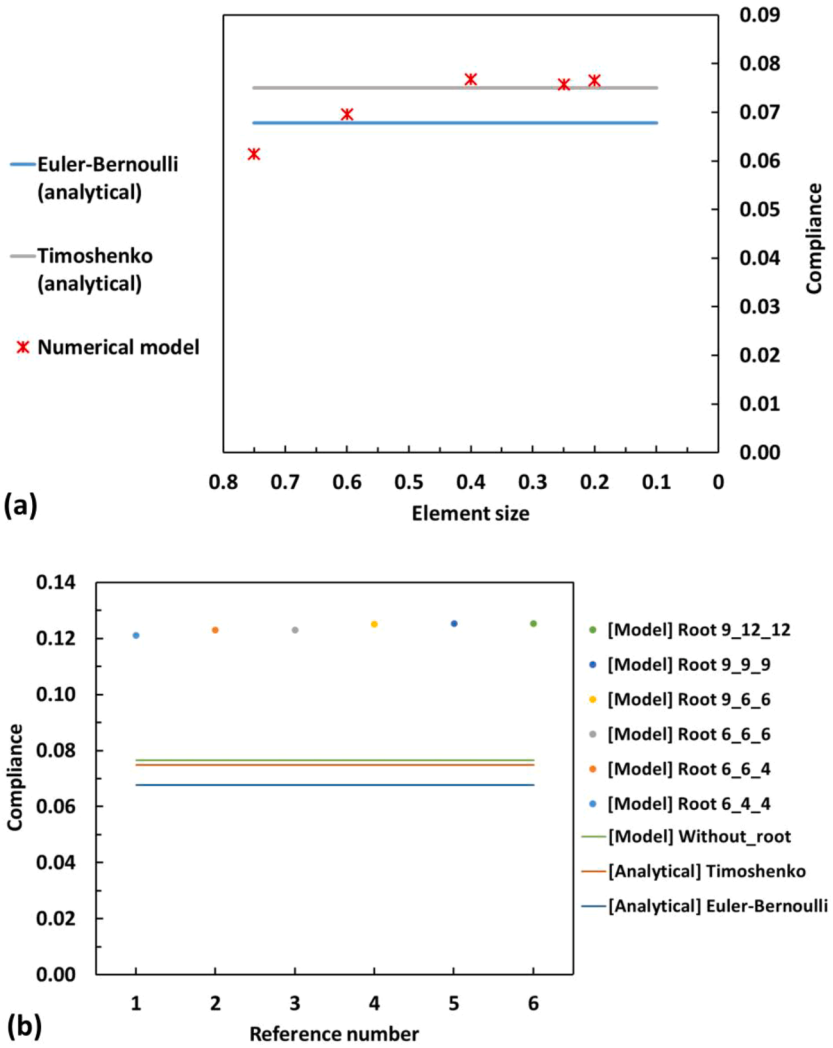

Fig. 3. (a) Compliance results (nm/μN) from numerical models with different mesh sizes (μm) are compared to that from analytical analysis based on Euler-Bernoulli and Timoshenko theories. Numerical models were constructed as rectangular beams with dimensions of width 3 μm, height 3 μm and effective length 8 μm, without beam root. The following uniform mesh sizes were tested: 0.75, 0.60, 0.40, 0.25, 0.20 μm. (b) Compliance results from numerical models with different dimensions of beam roots (referenced as ' [Model] Root 'height'_'width'_'length', the beams have the same dimensions as in (a)) and from analytical analysis based on Euler-Bernoulli and Timoshenko theories.

(Fig. 3*b*). It is therefore important to include beam roots in the models, especially for the case where the drift correction is enabled by the compliance evaluated numerically (e.g. monotonic test of sapphire in vacuum in the present study). For all the cantilever models in this paper, a 6 × 6 × 6 μm root was added to the fixed end of the cantilever, consistent with the size range in which little change was seen in Fig. 3b. The root had the same material properties as the beams and had all its free faces constrained with fixed displacement apart from the top surface.

3. Results

Chevron notched microcantilevers with pentagonal cross sections were fabricated on single crystal c-plane sapphire using FIB milling. These were aligned to fracture on either the a- or the m-plane.

Fig. 4*a-b* show an example of a cantilever prior to testing and its fracture surface after testing. All fractures, in air and in vacuum, occurred neatly at the chevron notch, with the fracture surfaces being almost perfectly smooth and flat and normal to the axis of the beam. No difference between regions of stable or unstable crack growth, nor the transition from one to the other, could be distinguished from the appearance of the fracture surfaces. The dimensions of each cantilever and the notches were retrieved from the corresponding high-resolution SEM images.

Each cantilever was coupled with a bespoke FE model to calculate the beam compliance during crack propagation as described in Section 2.4, using the dimensions measured experimentally (Fig. 4c-d). The compliances from 12 to 15 crack lengths were calculated numerically for each cantilever, with an individual sub-model created for each crack length to obtain the respective load-displacement responses. The numerical compliance was compared to that measured from the empirical load-displacement curves, exhibiting less than 10 % difference for all the cantilevers tested in the present study. The models were used to calculate crack lengths and stress intensity factors during the experiments.

3.1. Monotonic loading in air

Three sapphire cantilevers orientated for a-plane fracture and two for m-plane fracture (A1-A3 and M1-M2 respectively) were tested in air (Table 1). All samples exhibited stable crack growth up to the maximum load P_{max}.

The load-displacement curves for these cantilevers (Fig. 5*a*) were

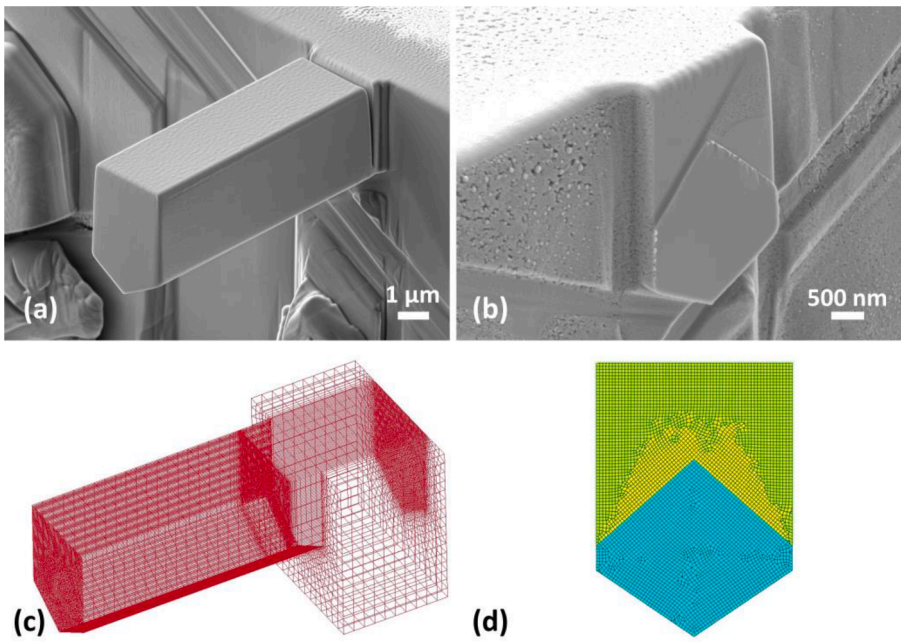

Fig. 4. (a) SEM image of a chevron-notched microcantilever with pentagonal cross section. (b) SEM image of fracture surface shown after the complete failure of cantilever in vacuum. (c) Numerical model of a chevron-notched microcantilever with pentagonal cross section. (d) Meshing of the chevron notch in the numerical model.

Table 1
Cantilever reference (#) and sample dimensions (W to L_n as defined in Fig. 2) for chevron-notched sapphire cantilevers tested in air, along with the measured maximum load (P_{max}), dimensionless factor for predicted normalised crack length at maximum load (α'_c), mean stable crack tip velocity (v), and stress intensity factor at the critical crack length $K_p(\alpha'_c)$. The average values for a- and m-plane fracture are expressed with standard error.

#	W μm	H μm	a_0 μm	a_1 μm	a_2 μm	L μm	L_n μm	P_{max} μN	α'_c	v m/s	$K_p(\alpha'_c)$ MPa$\sqrt{m}$	$\bar{K}_p(\alpha'_c)$ MPa$\sqrt{m}$
A1	2.90	2.71	1.37	2.50	0.97	7.15	0.92	231	0.15	2.8×10^{-8}	1.71	1.74±0.05
A2	2.87	3.14	1.48	2.78	0.83	7.01	1.13	276	0.16	2.9×10^{-8}	1.83	
A3	3.36	3.16	1.69	3.08	1.06	7.04	1.02	285	0.13	3.6×10^{-8}	1.67	
M1	2.71	2.79	1.35	2.51	0.73	7.31	1.05	207	0.16	2.6×10^{-8}	1.91	1.83±0.08
M2	2.61	2.93	1.45	2.54	0.74	7.13	0.91	211	0.13	2.1×10^{-8}	1.75	

linear during initial elastic loading, with crack propagation being revealed by the onset of nonlinear extension. The ensuing load-displacement curves were not perfectly smooth, showing variations in gradient. These corresponded to variations in the rate of crack growth as is shown in the crack length vs time plots in Fig. 5*b*. All the cracks propagated at average velocities in the range 2.1 – 3.6 × 10^{-8} m/s (Table 1) during the stable region of crack growth between crack initiation and the acceleration towards final failure.

Despite the variations in crack velocity, the K_p values during crack propagation (Fig. 5*c*), remained constant to within ~0.1 MPa $m^{1/2}$ for each individual specimen during the stable region of crack growth and all values recorded were in the range 1.6–1.9 MPa $m^{1/2}$. The K_p values at the normalised crack length α'_c for maximum load predicted by the models are shown in Table 1.

Although the nanoindenter was nominally under displacement control, crack growth rapidly accelerated to failure shortly after α'_c was exceeded, as is shown by the increasing spacing of the data points in Fig. 5c, which were collected at a constant rate. This was because the nanoindenter used for the tests in air is essentially a load-controlled machine with a feedback loop to approximate displacement control. This did not have a sufficiently short response time to reduce the load on the timescale required to maintain stable crack growth beyond the critical point. The close correspondence between the predicted values of α'_c in Table 1 and the experimental points of instability in Fig. 5c demonstrates the accuracy of the modelling.

3.2. Monotonic loading in vacuum

In vacuum, two sapphire cantilevers orientated for a-plane fracture were loaded continuously until complete failure (Table 2).

SEM images were taken every 2 s to record the loading behaviour of the cantilevers. Six SEM images from the loading process of cantilever AV2 are correlated with the corresponding loading curve in Fig. 6. The loading process can be summarised in three segments: (I) Points *a* to *b*: load increases linearly from zero as the cantilever bent elastically, followed by stable crack growth with the crack advancing to the point of maximum load *b*. The propagation of the crack cannot be observed clearly from the side of the notch due to small opening. (II) Points *b* to *c*: Crack continues to propagate stably thanks to the high stiffness and stability of the intrinsically displacement controlled nanoindenter used for the *in situ* tests, with the load eventually decreasing stably to very small values and the notch exhibiting further gradual opening. (III) Points *c* to *f*: Crack propagation remains stable throughout the rest of the fracture process, with the load remaining at around a few μN until the complete failure of the cantilever around point (e).

The indenter tip moved up and down its vertical axis during loading. For extreme displacements close to complete fracture shown in Fig. 6 (d)–(f) this meant that the tip moved noticeably relative to the beam but for the small displacements over which quantitative analysis was made ($a \leq a_1$ in Fig. 2a), the distance between the tip and the notch (L in Fig. 2a) varied by only ~1 %.

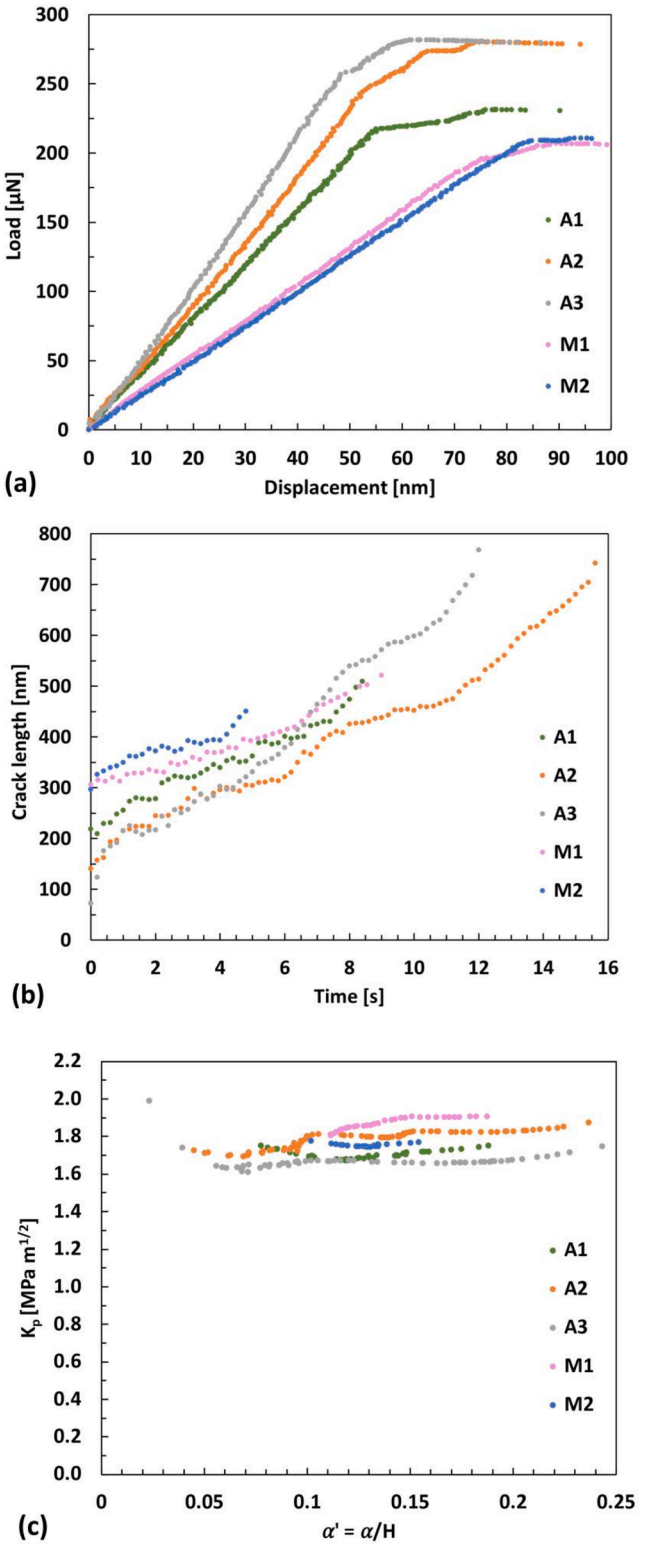

Fig. 5. (a) Load-displacement curves, (b) crack length vs time for cantilevers A1-A3 and M1-M2. Time=0 indicates the beginning of crack propagation. (c) Stress intensity factors measured during stable crack propagation.

The loading behaviour of both sapphire cantilevers tested monotonically was very similar, in terms of both loading curves (Fig. 7*a*) and the stable crack propagation recorded by SEM imaging. The load-displacement curves featuring the elastic bending and the early stage of stable crack growth are displayed with an expanded displacement scale in Fig. 7*b* to visualise the loading behaviour around Point *b*.

The K_p values at α'_c gave an average value of 2.76 ± 0.11 MPa m$^{1/2}$, which is significantly higher than the value of 1.74 ± 0.05 MPa m$^{1/2}$ measured in air. K_p measured during the stable crack propagation (Fig. 7*c*) indicates that the crack growth became stable at around $\alpha' = 0.1$ after the 'pop-in' event, with the measured K_p remaining approximately constant thereafter. The analysis was performed up to $\alpha' \approx 0.4$ corresponding to the end of the notch (i.e. while $a \leq a_1$ in Fig. 2a), beyond which the compliance of the cantilever was not evaluated using numerical models. The rate of crack propagation was approximately constant at 2.1–2.2 × 10^{-8} m/s (Table 2), as measured from the gradients of the plots in Fig. 7*d*.

3.3. Cyclic loading in vacuum

Cantilever AV4 (W = 3.0 μm, H = 3.44 μm, a_0 = 1.52 μm, a_1 = 3.01 μm, a_2 = 0.91 μm, L = 9.07 μm, L_n = 0.48 μm) was tested under cyclic loading in vacuum. Loading was retracted completely after the crack had propagated stably for a short distance, followed by re-loading to advance the crack further and unloading again. A total of 6 loading cycles were performed with the cantilever being loaded to complete failure in the final cycle. As shown in the load-displacement curves in Fig. 8, a sharp pop-in event during the 1st loading cycle was followed by stable crack extension. Unloading took place at a crack length of 862 nm. During the subsequent loading cycles, the load first increased linearly with the same slope as for the initial cycle 1 loading, showing that the crack had healed up along its full length. However, re-propagation of the crack began at a progressively lower load during each subsequent cycle, with the load eventually re-joining and continuing the previous curve from close to the point at which unloading had commenced.

After pop-in, K_p during cycle 1 was approximately 2.7 MPa m$^{1/2}$ during stable crack growth, in agreement with the monotonically loaded specimens. K_p values measured during crack propagation in loading cycles 1–4 are shown in Fig. 9 and the crack lengths as a function of time are shown in Fig. 10 (loading cycles 5 and 6 were not analysed here because the crack had propagated beyond the extent of the notch so the compliance calibration curve was no longer valid). Figs. 9, 10 show that for each of the re-loading cycles 2–4, the crack re-initiated at a lower $K_{p(healed)}$ than in cycle 1, becoming lower still with each successive cycle (from ≈1.6 MPa m$^{1/2}$ in Cycle 2, to ≈1.2 MPa m$^{1/2}$ in Cycle 3, then ≈1.0 MPa m$^{1/2}$ in Cycle 4). The re-initiated crack then grew with an increasing $K_{p(healed)}$ value until attaining the length reached during the previous cycle, at which point the crack arrested. During this re-fracture of the healed material, $K_{p(healed)}$ for a given crack length reduced with the number of previous healing cycles experienced. After crack arrest, the applied stress intensity factor gradually increased as loading continued and crack propagation began again when the K_p value of pristine material was reached. This exhibited highly consistent values around 2.6 to 2.7 MPa m$^{1/2}$, similar to that obtained in the monotonic tests beyond α'_c (Fig. 7c). Regardless of whether the crack propagation was in healed or pristine material, the crack velocities exhibited similar values between 1.9 × 10^{-8} and 2.2 × 10^{-8} m/s while propagating.

The unloading parts of the cycle in Fig. 8 show considerable hysteresis although the displacement always returned to close to zero when unloading was complete. Possible reasons for this are discussed in Section 4.2.

4. Discussion

4.1. Slow crack growth in alumina and comparison to literature values of K_p

As measured in the present study, the stress intensity factor for crack propagation K_p on the a-plane of sapphire in vacuum was 2.76 ± 0.11 MPa m$^{1/2}$, while the corresponding value in air was around 37 % lower at 1.74 ± 0.05 MPa m$^{1/2}$, showing unequivocally that K_p measured in air

Table 2
Details of a-plane chevron-notched sapphire cantilevers tested by monotonic loading in vacuum. Quantities as for Table 1.

#	W μm	H μm	a_0 μm	a_1 μm	a_2 μm	L μm	L_n μm	P_{max} μN	α'_c	v m/s	$K_p(\alpha'_c)$ MPa$\sqrt{m}$	$\bar{K}_p(\alpha'_c)$ MPa$\sqrt{m}$
AV1	3.22	3.31	1.54	3.07	0.99	9.20	0.64	442	0.16	2.2×10^{-8}	2.87	2.76±0.11
AV2	3.11	3.43	1.54	3.00	0.97	9.01	0.59	471.9	0.14	2.1×10^{-8}	2.65	

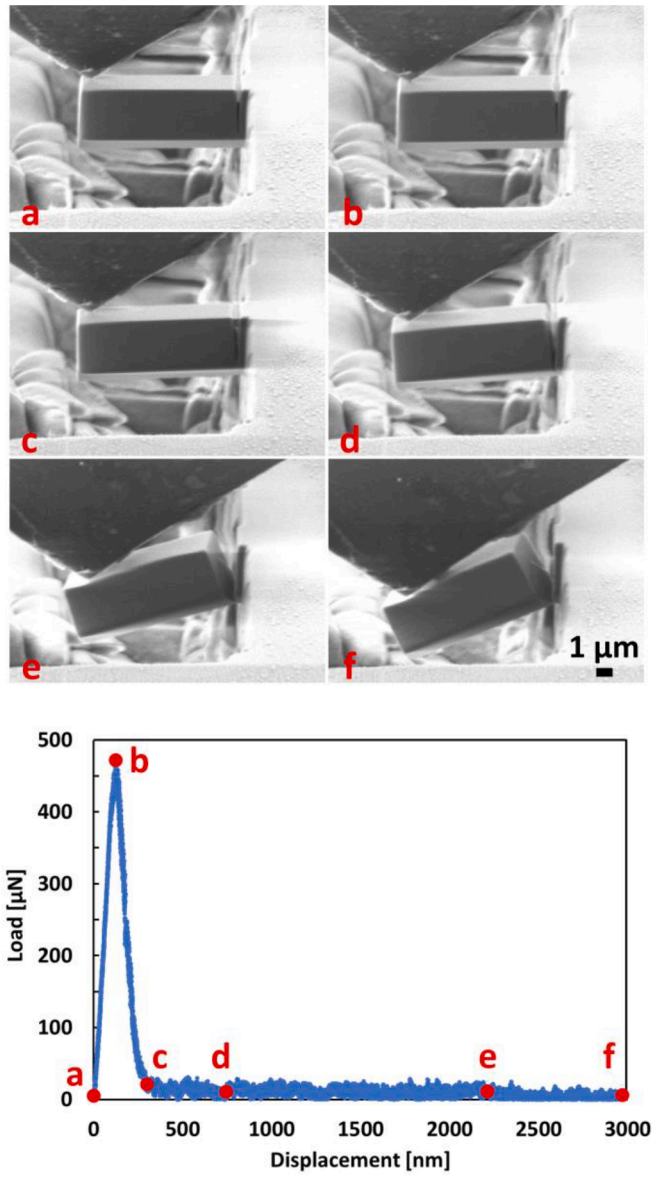

Fig. 6. SEM images and loading curve of cantilever AV2. The red dots correspond with the SEM images with the same letter.

was significantly affected by moisture-assisted SCG, as would be expected from the literature on macroscopic specimens. Moreover, the crack velocities measured in air ~ 10^{-8} m/s were at the lower end of Region I of SCG in Fig. 1, where the reduction in K_p is greatest according to macroscopic measurements on sapphire [39]. Therefore, our K_p values obtained in air are considered to be close to the threshold stress intensity factor for SCG K_0 for this environment, while K_p measured in vacuum was considered close to $K_{c(G)}$.

K_p data from published literature and the present study are summarised in Table 3. They exhibit wide variations, which is presumed to be mainly due to difficulties of investigating low crack growth rates, especially with macroscopic specimens, the use of different testing methods and procedures, and variations in humidity. Nevertheless, the overall trend demonstrates that fracture of sapphire is affected by moisture-assisted SCG: in comparison to apparent K_p values measured in air, the exclusion of moisture by testing in oil/vacuum/inert gas significantly increases K_p, whereas testing under water reduces it.

When a test is conducted in an environment where moisture is completely excluded, like oil, perfect vacuum or 100 % inert gas, K_p is in Region III of the SCG curve (Fig. 1) and is therefore between $K_{c(G)}$ and $K_{c(f)}$ [8,17]. K_p for the *a*-plane measured in the SEM vacuum chamber (~ 5 × 10^{-4} Pa) in the present study (2.76 ± 0.11 MPa $m^{1/2}$) was consistent to within experimental error with the generally accepted value measured in oil using macroscopic specimens by Iwasa and Bradt [40] (3.14 ± 0.30 MPa $m^{1/2}$). This gives confidence in our measurement method and demonstrates that a good vacuum was achieved in the SEM. Our value is at the lower edge of Iwasa and Bradt's rather broad error range, however, and this may reflect our very low crack growth rate bringing us closer to the threshold value $K_{c(G)}$ in Fig. 1 than the faster fracture conditions of Iwasa and Bradt and other previous reports. It is not yet clear how low a strain rate is required to approach the threshold value in vacuum but it is evident that the present method provides the means to investigate $K_{c(G)}$ and Region III of SCG more fully than has been possible to date.

The literature K_p values in Table 3 measured in dry nitrogen are significantly lower than those measured in vacuum and oil, which may be due to the difficulty of completely excluding moisture from commercial nitrogen [42].

Most of the *m*-plane K_p values in Table 3 are slightly higher than their comparable *a*-plane counterparts and that is true for our results in air as well, though the difference is at the limits of the experimental spread. Our crack growth rates are as low as is reasonably achievable with macroscopic specimens, and our K_p values may be close to the threshold value K_0 [8,9]. Our values at 54 % relative humidity (≈1.8 MPa $m^{1/2}$ for a- and m-planes) lie slightly above Salem's "recommended" threshold value for *a*- and *m*-plane sapphire at 85 % humidity of 1.65 MPa $m^{1/2}$, which is consistent with the accepted dependence of K_0 on humidity. Our values are on the lower end of the experimental range for K_p measured at 50 % relative humidity by Salem [24] on the a-plane using macroscopic pre-cracked beam and chevron notch specimens (2.06 ± 0.21 MPa $m^{1/2}$). This is consistent with the lower crack growth rates expected for our microcantilever tests.

Our values are less consistent with some of the other values in Table 3. However, K_p is likely significantly overestimated by Mitamura and Wang [41] (2.33 ± 0.07 MPa $m^{1/2}$) due to the relatively blunt saw notch (tip radius = 0.1 mm) employed in their macroscopic measurements, and it is not clear which Region of SCG their conditions lay in. The K_0 values reported by Norton et al. [16] (1.4 ± 0.2 MPa $m^{1/2}$) using straight notched microcantilevers involve significant corrections for FIB implantation stresses and notch bluntness, which might have resulted in systematic errors.

Although using the same chevron-notched microcantilever technique, the K_p values measured for nanocrystalline alumina by Mueller et al. [26] in air (2.34 ± 0.15 MPa $m^{1/2}$) are significantly higher than that measured in the present study in a similar environment, despite the fact that their fracture was intergranular, which, in fine grained alumina, is usually associated with slightly lower toughness values than the transgranular fracture corresponding to our single crystals, even when the effects of crack deflection are accounted for [43]. In addition,

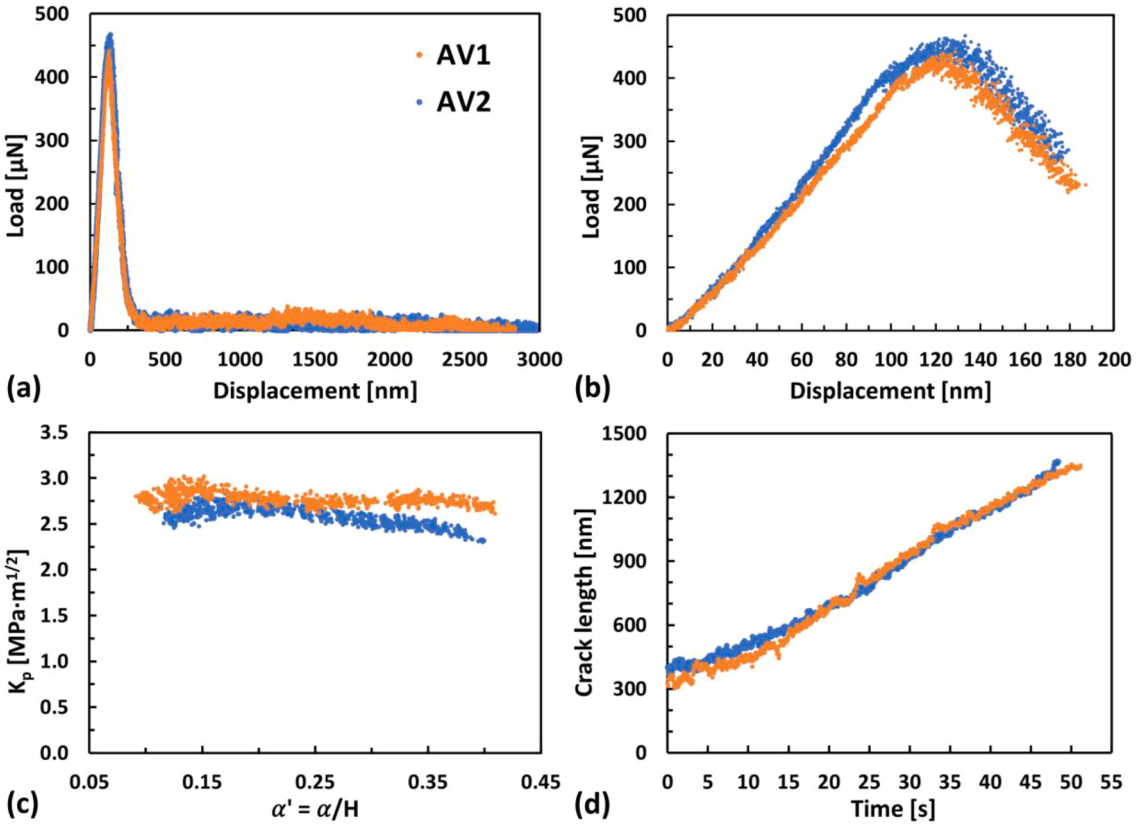

Fig. 7. Results for monotonic loading in vacuum, (a) entire load-displacement curves, (b) initial part of load-displacement curves with expanded displacement scale, (c) stress intensity factors measured during stable crack propagation and (d) curves of crack lengths as a function of time. Time = 0 indicates the beginning of crack propagation.

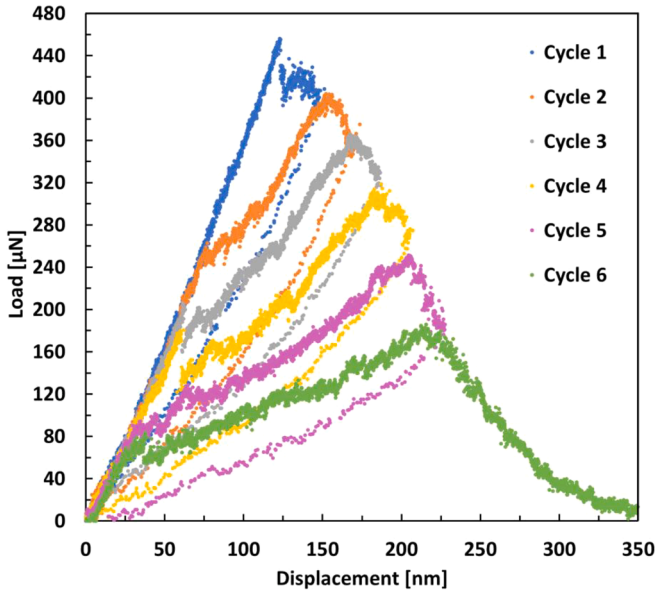

Fig. 8. Load-displacement curve of cantilever AV4, with cyclic loading in vacuum. A correction for displacement drift of +0.11 nm/s was applied (see Section 2.2). For loading cycle 6, the results at very low load before final failure (analogous to point c in Fig. 7) are omitted in order to optimise the visualisation of the rest of the curve.

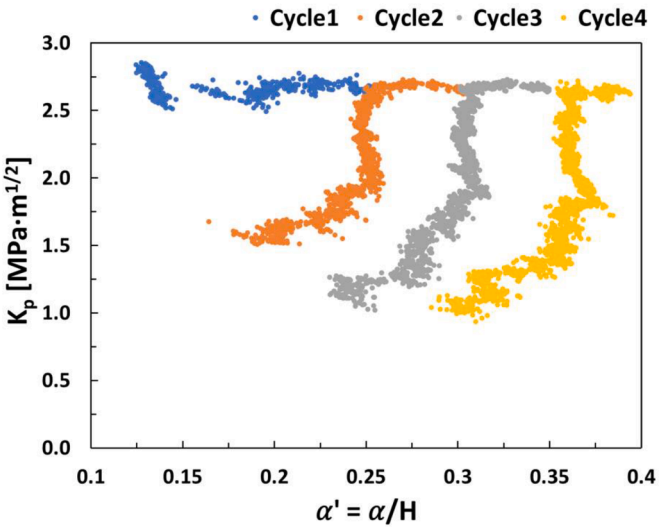

Fig. 9. Stress intensity factor K_p measured during stable crack propagation in a-axis sapphire cantilever tested in vacuum.

the loading rates in Ref. [26] (1–3 μN/s) are slightly lower than ours in the elastic region (5–11 μN/s) and, as pointed out by Žagar et al. [15], are so low that SCG should be dominant. The toughness values in Ref. [26] are calculated from the maximum load alone. The additional information in our investigation concerning crack velocities and instantaneous K_p values, comparison between environments with and without moisture, and quantitative agreement with previous work on

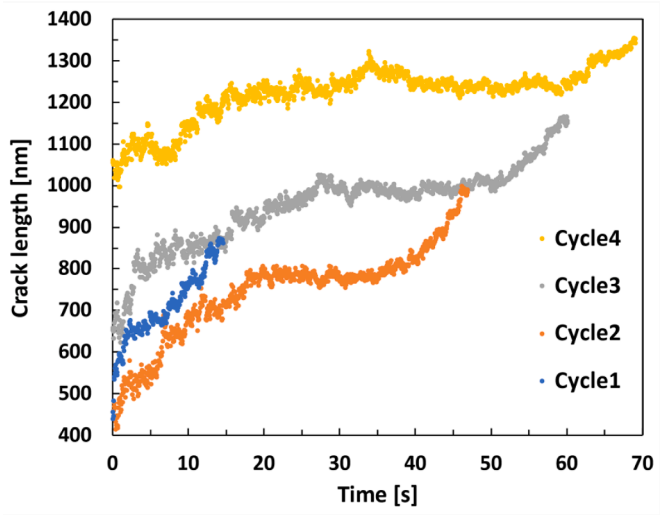

Fig. 10. Crack length as a function of time during crack propagation in the loading portion of each loading cycle for sapphire cantilever AV4 tested in vacuum. Time = 0 indicates the beginning of crack propagation in each cycle, i.e. it is reset for each cycle.

Table 3
K_p values measured for Al_2O_3.

Environment	Fracture plane	Testing scale	Crack rate [++]	K_p [MPa $m^{1/2}$]	Source
vacuum	a-plane	micro	10^{-8} m/s	2.76 ± 0.11	Present study
oil	a-plane	macro	/	3.14 ± 0.30	Iwasa and Bradt [40]
	m-plane	micro	F	3.5 ± 0.2	Norton et al. [16].
dry nitrogen	a-plane	macro	S	2.31 ± 0.12	Salem [24]
	m-plane	macro	10^{-4} m/s	2.59 ± 0.29*	Wiederhorn [25]
air	a-plane	micro	10^{-8} m/s	1.74 ± 0.05	Present study
	a-plane	macro	S	2.06 ± 0.21	Salem [24]
	a-plane	micro	F	1.4 ± 0.2	Norton et al. [16].
	m-plane	micro	10^{-8} m/s	1.83 ± 0.08	Present study
	m-plane	micro	F	1.5 ± 0.2	Norton et al. [16].
	m-plane	macro	F	2.33 ± 0.07	Mitamura and Wang [41]
	Nano-crystalline	micro	S	2.34 ± 0.15	Mueller et al. [26].
water	m-plane	micro	F	0.9 ± 0.2	Norton et al. [16].

[++] 'F' denotes fast fracture. For stable fracture, if the crack velocity is reported, it is noted as the scale on which the crack velocity is, in the unit of m/s. If the crack velocity is not reported, 'S' is applied to denote slow/stable fracture.

[*] The value is converted from the m-plane fracture energy 7.3 J/m^2 as reported in the reference and based on the assumption of isotropy and E = 430 GPa.

macroscopic test pieces strongly suggest that our measurements have observed and characterised SCG in microcantilevers.

Although the compliance criterion for a valid toughness test of Žagar et al. [15] checks that the maximum load occurs close to the crack length at which unstable crack propagation would begin in fast fracture, we note that the analysis does not allow for a threshold region of SCG (R_0 in Fig. 1). Fracture near the threshold would yield similar characteristics to fast fracture in that no crack propagation occurs below a threshold, K_0 or $K_{c(G)}$ according to the regime of fracture, followed by a very rapid acceleration of crack growth above it. Region II of SCG in sapphire under similar relative humidity to ours begins at crack velocities of ~10^{-5} m/s [39], three orders of magnitude faster than in the stable part of our tests. At sufficiently slow loading rates such as ours, therefore, relatively rapid, though still "sub-critical", fracture would also begin at the critical crack length beyond which K increases at constant load, as observed. The compliance test for fast fracture of Žagar et al. [15] is therefore not sufficient for practical microcantilever testing. The high values of K_p calculated from their results by Mueller et al. remain to be explained, nonetheless. In addition to more results under different testing conditions for the unusually fine-grained microstructure tested, another area worthy of exploration would be the sensitivity of the results to the meshing of their FE models. Full details of our FE optimisation are given in Section 2.4.

In summary, our measurements using stable crack growth in microscopic specimens avoid the problems of blunt notches, macroscopic test pieces and other experimental problems and the associated modelling is optimised the ensure accurate predictions. They also provide a clear contrast in behaviour between environments. The results demonstrate high reproducibility in terms of K_p and, crucially, allow an accurate value of the crack growth rate to be measured with very low crack tip velocities. The ability of microcantilevers to provide precise measurements under these conditions should enable SCG to be studied with more certainty then hitherto.

4.2. Crack healing and strength degradation

During the cyclic loading test, as the crack propagated further by the end of each loading cycle, the longer crack length resulted in an increase of cantilever compliance. However, the gradient of the linear part at the beginning of each cyclic loading curve exhibited a good match with that from the 1st cycle (as shown in Fig. 8), indicating that the compliance remained the same during the elastic bending at the beginning of each loading cycle. This demonstrates that the fracture surface retreated and healed itself over its full length after removal of the external load, which was enabled by the self-healing capability of alumina [30–32].

Although the crack reversibility in alumina has been observed *via* TEM examination [32], with cracks initiated by indentation exhibiting spontaneous closure and healing, this is the first time that quantitative toughness measurements of the extent of the healing have been made to our knowledge. Fig. 9 indicates that re-fracture of the healed material required a lower K_p ($\leq$ 1.6 MPa $m^{1/2}$) than that needed to propagate the crack in the pristine material (≈2.8 MPa $m^{1/2}$), demonstrating that the material did not fully recover its toughness during the self-healing process. Though the degradation was substantial, the toughness reduction of less than 50 % suggests that some primary bonding along the crack path (as opposed to weak secondary bonds such as Van der Waals forces) was restored during healing.

One potential explanation for the toughness degradation is mechanical frustration of closure caused by cleavage steps or other geometrical imperfections in the fracture plane [32,44,45]. Although such features were not apparent over most of the fracture surfaces at the resolution of SEM micrographs (Fig. 4b), some hackle that could have hindered closure of the crack is evident close to the top right hand edge of the fractured ligament. Any asymmetry in loading between the opening and closing part of the cycle could also have led to imperfect lattice matching leading to stacking faults and dislocation arrays [32]. Alternatively, surface reconstruction after fracture may not have allowed complete rebonding, and chemical species [31] (such as gas molecules, carbon contamination, etc.) in the SEM chamber might have adsorbed on the crack faces, and then been incorporated in the sapphire as the crack healed. It is notable (i) that $K_{p(healed)}$ at a given crack length decreased with the increasing number of times the interface had healed (Figs. 8, 9), and (ii) that $K_{p(healed)}$ increased as the crack progressed along the previously healed path (Fig. 9). Though interesting, these observations can be explained either in terms of the mechanical/geometrical mechanism, in which mismatch would be more severe for the parts of the crack faces further behind the crack tip position at the beginning of the closure cycle, or in terms of the surface reconstruction/chemical

adsorption mechanisms, which would be more severe for the crack surfaces that had been exposed for the longest time. These two explanations could be distinguished in future experiments by incorporating dwells of various durations in the cycles as well as by microstructural examination using TEM-based methods.

If the crack growth were perfectly reversible, corresponding to an equilibrium state for each displacement, the unloading curves in Fig. 8 would retrace the path of the envelope representing crack growth through previously uncracked material. Alternatively, if classical linear elastic fracture mechanics were obeyed for crack extension but healing did not occur, the load displacement curves would simply follow a straight line back to the origin on unloading. The hysteresis evident in Fig. 8 is more pronounced than this, however, with the initial gradient of the curves on load reversal following a steeper trajectory. Elastic cycling of un-notched silicon beams did not show this effect and the videos of the sapphire tests did not show evidence of indenter slippage or distortion of the beam sufficient to explain the hysteresis, so this does not appear to be an artefact of the loading system.

One potential explanation is that premature crack closure occurs due to surface roughness [46] as described above in connection with healing. The gradients of the load displacement curves on unloading are initially similar to those immediately before the crack starts to grow through new material in the same cycle, implying that closure would need to have occurred over the length of newly formed crack, 100–200 nm in these experiments. The separation of the crack faces at this distance behind the crack tip at fracture is ~8 nm according to the Irwin crack profile. However, although the depth of the hackle noted above in Fig. 4(b) is consistent with this, it is at one edge of the fractured ligament and most of the fractured area appears very flat and smooth, so the crack would not be completely prevented from closing on load reversal as required to explain the results. A further possibility is that chemisorbed species from the SEM atmosphere act to wedge open the crack [47,48] but the scale of the above crack opening needing to be "wedged" is much greater than the thickness of adsorbed layers and related effects [48]. Significant premature crack closure therefore seems unlikely.

The hysteresis can also be explained if the crack continues to grow during the initial part of the unloading, reducing the compliance and therefore the load for a given displacement, as observed. If K_p at the point of load reversal remained slightly higher the $K_{c(G)}$, this would be consistent with Region III of SCG and the observed crack growth rates during the loading portion of the curve (~20 nm/s) would be sufficient to provide an increase in compliance of the right order if continued during the first few seconds of unloading. We therefore tentatively attribute the hysteresis to near-K_c SCG. This clearly deserves further investigation but, as noted above, this method offers a suitable means to investigate not only Region I of SCG but also the seldom investigated Region III.

5. Conclusions

Stress intensity factors for crack propagation K_p on the *a*- and *m*-planes of sapphire were measured using chevron-notched microcantilevers, in vacuum (*in situ* SEM) and in air, and in monotonic and cyclic loading. Stable crack growth enabled K_p to be measured reliably and continuously, free from the complicating effects of FIB damage at notch tips and notch bluntness commonly encountered in fast fracture of microscopic specimens.

K_p measured in vacuum, where moisture was excluded, was considered to be close to the equilibrium fracture toughness K_c with a value of 2.8 ± 0.1 MPa $m^{1/2}$ for *a*-plane sapphire.

K_p measured in air at 54 % relative humidity was decreased substantially by moisture-assisted slow crack growth and was considered close to the threshold stress intensity for SCG, K_0. For sapphire, the K_0 values for *a*- and *m*-planes were close to each other, at 1.74 ± 0.05 and 1.83 ± 0.08 MPa $m^{1/2}$ respectively. The crack velocities were approximately 20 nm/s, corresponding to the lower end of Region I of the SCG curve. Accurate measurements of SCG characteristics are essential to the reliable long term application of ceramic components but are difficult to measure accurately using macroscopic specimens. The method employed here provides an accurate means of achieving this without the long timescales required in macroscopic tests.

Cyclic loading in vacuum showed that cracks healed spontaneously over their full length on load removal at room temperature. However, the toughness of the healed interfaces was found to be progressively degraded by repeated cycling, from 2.8 MPa $m^{1/2}$ for virgin *a*-plane sapphire to 1.6 MPa $m^{1/2}$ after 1 healing cycle and to 1.0 MPa $m^{1/2}$ after 3 cycles. This represents the first fully quantitative investigation of the degradation of toughness after healing, which was thought to be due to an incomplete restoration of the lattice across the separation interface, possibly aided by the incorporation into the sapphire of species from the SEM atmosphere adsorbed onto the crack faces.

The method has wide applicability for the fundamental science and accurate measurement of slow crack growth and crack healing in different environments. It can be used to investigate not only single crystals and amorphous materials but also individual microstructural features such as grain boundaries and other interfaces.

Supplementary material

The following videos are available as Supplementary Material related to this article.

Video S1. Monotonic loading of cantilever AV1.

Video S2. Monotonic loading of cantilever AV2.

Video S3. Cyclic loading of cantilever AV4.

CRediT authorship contribution statement

Jiawei Jiang: Conceptualization, Data curation, Formal analysis, Investigation, Methodology, Visualization, Writing – original draft. **Simone Falco:** Formal analysis, Investigation, Methodology, Software, Validation, Writing – original draft. **Siyang Wang:** Investigation, Methodology, Writing – review & editing. **Finn Giuliani:** Resources, Writing – review & editing. **Richard I Todd:** Conceptualization, Formal analysis, Funding acquisition, Methodology, Project administration, Resources, Supervision, Writing – original draft, Writing – review & editing.

Declaration of competing interest

The authors declare that they have no known competing financial interests or personal relationships that could have appeared to influence the work reported in this paper.

Acknowledgements

J. Jiang, S. Falco, R. I. Todd and this work were financially supported by the Defence Science and Technology Laboratory (Dstl) of the UK Ministry of Defence [grant number DSTL/AGR/00507/01]. The contributions of D. E. J. Armstrong in providing the *ex-situ* nanoindenter and in the experimental techniques involved in the testing of microcantilever beams are gratefully acknowledged. The authors acknowledge use of characterisation facilities within the David Cockayne Centre for Electron Microscopy, Department of Materials, University of Oxford, alongside financial support provided by the Henry Royce Institute (Grant ref EP/R010145/1). The authors are grateful to one of the reviewers for emphasising the physical importance of threshold stress intensity factors.

Supplementary materials

Supplementary material associated with this article can be found, in the online version, at doi:10.1016/j.actamat.2024.119914.

References

[1] F.S. Hannon, K.H. Abbott, Ceramic armor stops bullets, lowers weight, Mater. Eng. 68 (1968) 42–43.
[2] R.F. Rolston, E. Bodine, J. Dunleavy, Breakthrough in armor, Space Aeronaut. 50 (1968) 55–63.
[3] D. Schmitz, The history of armor, Iowa Rev. 10 (1979), 105-105.
[4] S.R. Skaggs, A brief history of ceramic armor development, in: Proceedings of the 27th International Cocoa Beach Conference on Advanced Ceramics Composites, Cocoa Beach, Fl, 2003, pp. 337–349.
[5] P.J. Hazell, Ceramic Armour: Design and Defeat Mechanisms, Argos Press, Canberra, Australia, 2006.
[6] P.G. Karandikar, G. Evans, S. Wong, M.K. Aghajanian, M. Sennett, A review of ceramics for armor applications, in: Proceedings of the 32nd International Conference on Advanced Ceramics and Composites, Daytona Beach, FL, 2008, pp. 163–175.
[7] A.G. Evans, Slow crack growth in brittle materials under dynamic loading conditions, Int. J. Fract. 10 (1974) 251–259.
[8] B. Lawn, Fracture of Brittle Solids, Second Edition ed, Cambridege University Press, 1993.
[9] B.R. Lawn, An atomistic model of kinetic crack growth in brittle solids, J. Mater. Sci. 10 (1975) 469–480.
[10] A. Evans, H. Johnson, The fracture stress and its dependence on slow crack growth, J. Mater. Sci. 10 (1975) 214–222.
[11] T.J. Chuang, L. Chuck, R.J. Fields, E.R. Fuller, Effects of crack growth on the load-displacement characteristics of precracked specimens under bending, Eng. Fract. Mech. 18 (1983) 1099–1109.
[12] D. Munz, G. Himsolt, J. Eschweiler, Comparison of high-temperature fracture toughness of hot-pressed Si3N4 with straight-through and chevron notches, J. Am. Ceram. Soc. 63 (1980) 341–342.
[13] T.B. Troczynski, P.S. Nicholson, Effect of subcritical crack growth on fracture toughness and work-of-fracture tests using chevron-notched specimens, J. Am. Ceram. Soc. 70 (1987) 78–85.
[14] J. Sung, P.S. Nicholson, Valid K_{IC} determination via in-test subcritical precracking of chevron-notched bend bars, J. Am. Ceram. Soc. 72 (1989) 1033–1036.
[15] G. Žagar, A. Singh, V. Pejchal, M.G. Mueller, A. Mortensen, On measuring fracture toughness under load control in the presence of slow crack growth, J. Eur. Ceram. Soc. 35 (2015) 3155–3166.
[16] A.D. Norton, S. Falco, N. Young, J. Severs, R.I. Todd, Microcantilever investigation of fracture toughness and subcritical crack growth on the scale of the microstructure in Al_2O_3, J. Eur. Ceram. Soc. 35 (2015) 4521–4533.
[17] S.M. Wiederhorn, Moisture assisted crack growth in ceramics, Int. J. Fract. Mech. 4 (1968) 171–177.
[18] T.A. Michalske, B.C. Bunker, S.W. Freiman, Stress corrosion of ionic and mixed ionic/covalent solids, J. Am. Ceram. Soc. 69 (1986) 721–724.
[19] M. Ebrahimi, J. Chevalier, G. Fantozzi, Slow crack-growth behavior of alumina ceramics, J. Mater. Res. 15 (2000) 142–147.
[20] C. Olagnon, J. Chevalier, V. Pauchard, Global description of crack propagation in ceramics, J. Eur. Ceram. Soc. 26 (2006) 3051–3059.
[21] A. Krell, E. Pippel, J. Woltersdorf, W. Burger, Subcritical crack growth in Al2O3 with submicron grain size, J. Eur. Ceram. Soc. 23 (2003) 81–89.
[22] V.M. Sglavo, D.J. Green, Threshold stress intensity factor in soda-lime silicate glass by interrupted static fatigue test, J. Eur. Ceram. Soc. 16 (1996) 645–651.
[23] S.M. Wiederhorn, Fracture surface energy of glass, J. Am. Ceram. Soc. 52 (1969) 99–105.
[24] J.A. Salem, Slow crack growth and fracture toughness of sapphire for the international space station fluids and combustion facility, Glenn Res. Center (2006). NASA Cleveland, Ohio.
[25] S.M. Wiederhorn, Fracture of sapphire, J. Am. Ceram. Soc. 52 (1969) 485–491.
[26] M.G. Mueller, V. Pejchal, G. Žagar, A. Singh, M. Cantoni, A. Mortensen, Fracture toughness testing of nanocrystalline alumina and fused quartz using chevron-notched microbeams, Acta Mater. 86 (2015) 385–395.
[27] A.D. Norton, Measuring and Understanding Grain Boundary Properties of Engineering Ceramics, DPhil Department of Materials, University of Oxford, Oxford, UK, 2013.
[28] T. Fett, D. Creek, S. Wagner, G. Rizzi, C.A. Volkert, Fracture toughness test with a sharp notch introduced by focussed Ion beam, Int. J. Fract. 153 (2008) 85–92.
[29] D. Picard, D. Leguillon, C. Putot, A method to estimate the influence of the notch-root radius on the fracture toughness measurement of ceramics, J. Eur. Ceram. Soc. 26 (2006) 1421–1427.
[30] Y. Yang, A. Kushima, W. Han, H. Xin, J. Li, Liquid-like, self-healing aluminum oxide during deformation at room temperature, Nano Lett. 18 (2018) 2492–2497.
[31] B.R. Lawn, D.H. Roach, R.M. Thomson, Thresholds and reversibility in brittle cracks: an atomistic surface force model, J. Mater. Sci. 22 (1987) 4036–4050.
[32] B.J. Hockey, B.R. Lawn, Electron microscopy of microcracking about indentations in aluminium oxide and silicon carbide, J. Mater. Sci. 10 (1975) 1275–1284.
[33] K. Minoshima, T. Terada, K. Komai, Influence of nanometre-sized notch and water on the fracture behaviour of single crystal silicon microelements, Fatigue Fract. Eng. Mater. Struct. 23 (2000) 1033–1040.
[34] D. Munz, R.T. Bubsey, J.L. Shannon, Fracture toughness determination of Al2O3 using four-point-bend specimens with straight-through and chevron notches, J. Am. Ceram. Soc. 63 (1980) 300–305.
[35] F.W. DelRio, R.F. Cook, B.L. Boyce, Fracture strength of micro- and nano-scale silicon components, Appl. Phys. Rev. 2 (2015) 021303.
[36] D.B. Hovis, A. Reddy, A.H. Heuer, X-ray elastic constants for α-Al_2O_3, Appl. Phys. Lett. 88 (2006).
[37] S. Falco, "Numerical modelling and experimental characterisation of mechanical performance of ceramic materials at multiple scales," DPhil, University of Oxford, 2015.
[38] D.E.J. Armstrong, A.J. Wilkinson, S.G. Roberts, Measuring anisotropy in Young's modulus of copper using microcantilever testing, J. Mater. Res. 24 (2009) 3268–3276.
[39] S.M. Wiederhorn, Fracture of ceramics. Mechanical and Thermal Properties of Ceramics, NBS Special Publication, 1969, pp. 217–241, ed. J. B. Wachtman Jr303.
[40] M. Iwasa, R. Bradt, Fracture Toughness of Single-Crystal Alumina in Advances in Ceramics vol. 10 (1984).
[41] Y. Mitamura, Y. Wang, Fracture toughness of single crystal alumina in air and a simulated body environment, J. Biomed. Mater. Res. 28 (1994) 813–817.
[42] A.C. Walker, E.J. Ernst, Moisture content of compressed nitrogen, Ind. Eng. Chem. Anal. Ed. 2 (1930) 139–140.
[43] Thomas Hansson, Richard Warren, J. Wasén, Fracture toughness anisotropy and toughening mechanisms of a hot-pressed alumina reinforced with silicon carbide whiskers, J. Am. Ceram. Soc. 76 (1993) 841–848.
[44] M. Swain, B. Lawn, S. Burns, Cleavage step deformation in brittle solids, J. Mater. Sci. 9 (1974) 175–183.
[45] J. Williams, B. Lawn, M. Swain, Cone crack closure in brittle solids, Phys. Status Solidi (a) 2 (1970) 7–29.
[46] R. Pippan, A. Hohenwarter, Fatigue crack closure: a review of the physical phenomena, Fatigue Fract. Eng. Mater. Struct. 40 (2017) 471–495.
[47] R. Thomson, The molecular wedge in a brittle crack - A simulation of mica water, J. Mater. Res. 5 (1990) 524–534.
[48] K.T. Wan, B.R. Lawn, Effect of chemical interaction on Barenblatt crack profiles in brittle solids, Acta Metall. Mater. 40 (1992) 3331–3337.